

1. STRUCTURAL OBSERVATIONS FROM THE CÔTE D'IVOIRE-GHANA TRANSFORM MARGIN¹

E.A. Pickett^{2,3} and S. Allerton²

ABSTRACT

Ocean Drilling Program Leg 159 to the Côte d'Ivoire-Ghana Transform Margin provided an invaluable opportunity to document the structures of a continental transform margin from the Albian to the present. Observations of core and thin sections, together with analyses of structural and bedding dip data, have led to a better understanding of the styles of deformation involved. The cores from all sites (959–962) display a wide range of deformation styles with the most intense concentration of faults, veins, and microfolds occurring toward the base of each site; possibly related to deformation during the syntransform stage. At Sites 959 and 960, the downhole increase in deformation coincides with the unconformity between Lower Cretaceous clastic sediments and overlying undeformed late Albian–Turonian carbonates. Normal faults are the most common fault type, whereas evidence for strike-slip is surprisingly rare. Veins are common throughout the successions and commonly display several generations of vein fill. At Site 959 a second deformation event has been recorded, affecting sediments below 750 meters below seafloor (early Eocene and older). Changes in physical properties of the sediments, vein compositions, and a decrease in bedding dip above this level indicate a decrease in tectonic activity at this time. A possible mechanism, which may have caused this change in tectonic regime, may be related to a switch from uncoupled to coupled linkage between the continental and oceanic crust.

INTRODUCTION

Regional Setting and Tectonic Framework of the Côte d'Ivoire-Ghana Transform Margin

The Côte d'Ivoire-Ghana Transform Margin was generated as a result of major transform displacement—initially between the continental plates of Africa and South America; subsequently, between the continental crust of Africa and oceanic crust of the Atlantic (Masclé and Blarez, 1987). The Côte d'Ivoire-Ghana Transform Margin represents a continuation of the oceanic Romanche Fracture Zone, whose active segment offsets the Mid-Atlantic Ridge. The Côte d'Ivoire-Ghana Margin is characterized by a northeast-southwest trending ridge that bounds the transform margin along the adjacent extensional Deep Ivorian Basin (Fig. 1). In this area, the continental shelf is separated from the adjacent oceanic abyssal plain by a steep, narrow continental slope, approximately 20–30 km in width. The Côte d'Ivoire-Ghana Marginal Ridge occurs along the transition between laterally thinned continental crust to the north and adjacent oceanic crust to the south.

The Marginal Ridge was the focus of drilling during Ocean Drilling Program (ODP) Leg 159, with the drill sites (Sites 959–962) forming an approximately northeast-southwest section along its strike (Fig. 1). The oldest rocks recovered comprise a series of tectonized Albian sedimentary rocks, which were deposited in a deep-water lacustrine setting. These sedimentary rocks may record an early phase of intra-continental transform motion between Africa and South America. The sequence passes upward into a progressively more marine succession that is interpreted as having been deposited in a pull-apart basin that developed as breakup continued. A present-day analogue is the Salton Trough associated with the San Andreas

fault zone in which there is a complex pattern of continental, lacustrine, and shallow-marine sedimentation (Crowell, 1974). After continental breakup, published tectonic models of transform margins predict that the phase of active ocean-continent transform movement is terminated by the migration of a spreading center along the margin (e.g., Masclé and Blarez, 1987; Basile et al., 1993). Heat transfer from the spreading center is predicted to produce a major phase of uplift. In this case, it has been inferred that this generated the Marginal Ridge during the Cenomanian–Turonian (Basile et al., 1993). Following the passage of the ridge, the margin is predicted to have undergone thermal subsidence with no further strike-slip activity. Models for the opening of the equatorial Atlantic suggest that rifting probably commenced in Neocomian–Aptian times, and that the spreading ridge passed by the Marginal Ridge in Late Cretaceous times (Masclé and Blarez, 1987). Turonian–Santonian reefal carbonates and high-energy, coarse clastic rocks are interpreted to have been deposited during uplift associated with this ridge passage. The deep-water black shale facies, recovered from Hole 959, are interpreted as recording deepening of the basin because of subsidence in response to subsequent cooling. However, structural and geochemical evidence from Leg 159 record the effects of a later, Eocene, event.

This paper is based on direct shipboard observations of cores and a short post-cruise study of samples and structural data. The purpose of this contribution is to provide a concise, largely descriptive account of the structures observed at Sites 959–962 (see also Benkhelil et al., Chap. 2, this volume) and to briefly discuss the results of an investigation of structural data obtained from the cores, including tilt rates for Site 959.

METHODS

Structures observed in the core were initially sketched and described on visual core description forms and, where possible, their orientations with respect to the core liner were measured. The orientations of bedding planes and other planar structures (e.g., faults and veins) were made by measuring two apparent dips to calculate a “true” dip in the core reference frame (see Shipboard Scientific Party,

¹Masclé, J., Lohmann, G.P., and Moullade, M. (Eds.), 1998. *Proc. ODP. Sci. Results, 159*: College Station, TX (Ocean Drilling Program).

²Department of Geology and Geophysics, Grant Institute, West Mains Road, Edinburgh EH9 3JW, United Kingdom.

³Present address: British Geological Survey, Murchison House, West Mains Road, Edinburgh EH9 3LA, United Kingdom. eapi@wpo.nerc.ac.uk

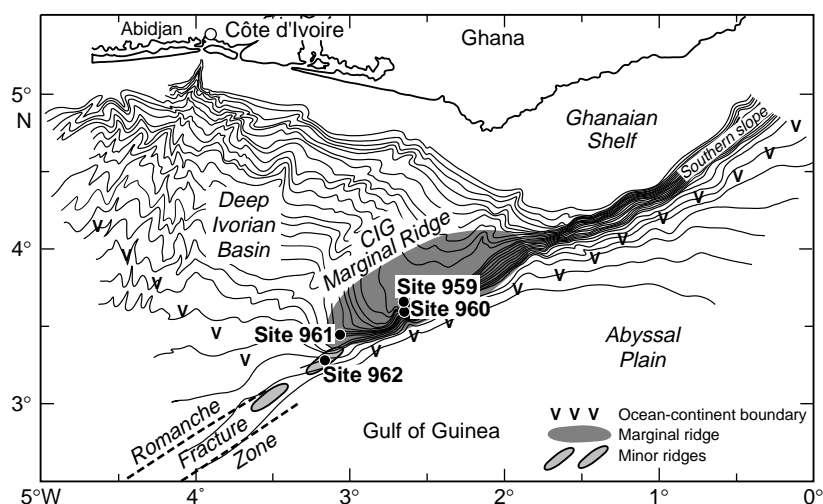


Figure 1. Location map showing simplified bathymetry and the main morpho-structural features of the Côte d'Ivoire-Ghana Transform Margin. The positions of the Leg 159 sites on the Marginal Ridge are also marked (after Mascle, Lohmann, Clift, et al., 1996).

1996a). An estimation of the declination errors inherent in this technique (assuming that the apparent dips can be measured to the nearest degree) indicates high errors for near-horizontal structures, but much lower errors for moderately dipping structures (Shipboard Scientific Party, 1996a). Linear structures, such as slickensides and mineral lineations, were measured either directly using their azimuth and amount of plunge, or by measuring the pitch of the structure from the strike of a previously measured plane.

Thin sections were also examined, both on ship and during post-cruise studies. This was particularly valuable for the study of veins, including the identification of vein minerals and the various generations of vein fill.

In poorly consolidated sediment cores, particular care was taken to try and ensure that the observed structures were true tectonic features and not caused by drilling. In many cases this was difficult, and ambiguous structures were recorded as possibly drilling induced, and were ignored for the purposes of this study. The need for careful observation of structures in cores was highlighted by Kopf and Flecker (1996). Their study of normal faults in cores recovered by the advanced hydraulic piston corer (APC) on ODP Leg 160 led them to suggest that tectonic faults are not easily distinguished from brittle failure induced by the APC technique.

In this paper only the amount of dip of structures is considered. As pointed out by Allerton (Chap. 20, this volume) no systematic reorientation scheme could be applied to the structural measurements owing to weakly magnetized rocks, drilling-induced remagnetizations, and limited Formation MicroScanner (FMS) log data.

SUMMARY OF STRUCTURES OBSERVED DURING LEG 159

Four sites were drilled during ODP Leg 159, all within continental crust adjacent to the continent-ocean transition of the Côte d'Ivoire-Ghana Margin (Fig. 1). Site 959 was drilled on the flanks of the Deep Ivorian Basin, a few kilometers north of the crest of the Marginal Ridge that runs parallel to the transform margin. Site 960 was located close to the top of the ridge. Site 961 was drilled at the western end of the Marginal Ridge close to the continent/ocean boundary of the Côte d'Ivoire-Ghana Margin. Site 962 targeted a small buried ridge extending toward the transition with the Romanche Fracture Zone. Figure 2 shows a summary diagram of the lithologic units recovered and the distribution of structures observed at the four sites (modified after Shipboard Scientific Party, 1996b). The following account summarizes the tectonic structures observed at Sites 959–962. For a sum-

mary of the soft-sedimentary deformation features observed, see Benkhelil et al. (Chap. 2, this volume).

Site 959

Site 959 is located at latitude 3°38'N, longitude 2°44'W in a water depth of 2100 m. It is situated on a small plateau, which extends just to the north of the crest of the Côte d'Ivoire-Ghana Marginal Ridge, on the southern shoulder of the Deep Ivorian Basin. Four holes were drilled (959A, 959B, 959C, and 959D) with a maximum penetration achieved in Hole 959D at 1159 meters below sea floor (mbsf).

Faults first appear at 92 mbsf in Hole 959A and 45 mbsf in Hole 959B and are common throughout the underlying sequence, with the exception of the porcellanites of lithologic Subunit IIC in which faults are relatively rare. The faults generally have a normal sense of displacement with offsets up to a few centimeters. Reverse faults are relatively rare and, where present, form minor accommodation structures within zones of predominantly normal faulting. The diatomites of lithologic Subunit IIC (within the interval 340–360 mbsf) are deformed by an anastomosing set of steeply dipping faults, which enclose lenses of sheared diatomite and are marked by thin seams of fine-grained, gray-colored gouge (Fig. 3). These are post-dated by a set of sharp, planar normal faults (offsets up to 1 cm) that dip at approximately 45°. These later faults do not contain fault gouge. Slickensides developed on these later fault surfaces indicate a dip-slip sense of displacement.

At 750 mbsf in Hole 959D, there is a marked increase in the intensity of deformation, occurring at approximately 62 m above the base of the porcellanites. This change also coincides with the appearance of quartz and calcite veins, with very few veins observed above 750 mbsf. Quartz veining observed at 758 mbsf takes the form of a series of chalcedony-filled tension gashes. However, the first significant occurrence of veining is within the porcellanite at 750.7 mbsf, where quartz appears as a septarian-type network of composite veins comprising three generations of syntaxial vein fill. In detail, the earliest generation of vein fill is a thin rim of fibrous chalcedony that locally grades into the wall rock. The second generation is characterized by a thicker layer (up to 0.25 mm) of botryoidal chalcedony. The boundary between these two generations of quartz is in some cases gradational. The youngest generation of vein fill is represented by a central zone of calcite, forming large, single crystals that display little or no evidence of intra-crystalline deformation. This change in vein mineralogy from quartz to calcite clearly indicates a change in fluid composition and/or temperature.

Veins containing calcite, kaolinite, pyrite, and barite were observed in the succession from 750 mbsf to the bottom of Hole 959D

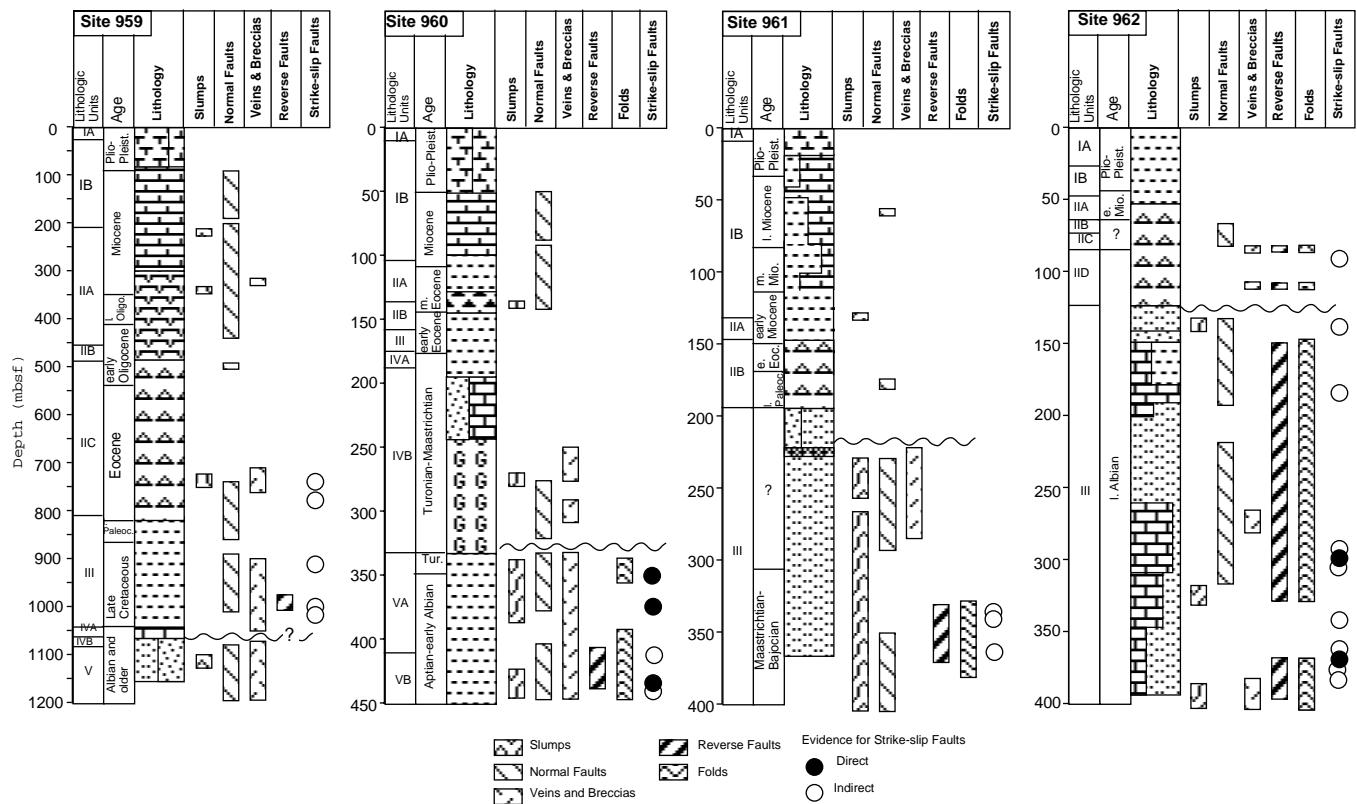


Figure 2. Summary diagram showing the main distribution of structures at Sites 959–962 (modified after Shipboard Scientific Party, 1996b). Lithologic symbols are from Shipboard Scientific Party (1996a). Evidence for strike-slip is shown as direct (horizontal or near-horizontal lineations and definite flower-type structures) or indirect (vertical or near-vertical shear zones, oblique lineations, and close association of normal and reverse faults).

at 1159 mbsf. A calcite-kaolinite-pyrite mineral association is common within the black claystones of lithologic Unit III (812–1043 mbsf). Pyrite is ubiquitous in this unit, occurring both as vein fill and within the wall rock as disseminated grains and discrete nodules. Barite veins were also observed in this lithologic unit where they are locally associated with asymmetric microfolds. At depth within Hole 959D (1081–1159 mbsf), calcite-kaolinite veins were observed in the quartz-rich sandstone and claystone of lithologic Unit V.

Evidence for strike slip at Site 959 is indirect, consisting mainly of vertical faults, some displaying oblique slickensides (e.g., Core 159-959D-35R), and close associations of normal and reverse faults (e.g., Cores 159-959D-39R and 59R). Near-vertical faults with oblique slickensides occur at ~740 mbsf in Hole 959D, providing indirect evidence for strike-slip motion. The next possible evidence for strike slip occurs between 903 and 1009 mbsf in Hole 959D. The structures observed in this interval include vertical to near-vertical faults and closely associated normal and reverse faults.

Site 960

Site 960 is located at latitude 3°35'N, longitude 2°44'W in a water depth of 2061 m. It is situated approximately 5 km south of Site 959 on a small plateau at the summit of the Marginal Ridge. Three holes were drilled (960A, 960B, and 960C) with a maximum penetration achieved in Hole 960A (451 mbsf).

In Hole 960A, deformation of the nanofossil/foraminifer oozes and chalks of lithologic Unit I (0–100 mbsf) is characterized by normal faulting, which displays offsets of up to 4 cm. The coarse carbonates of lithologic Subunit IVB appear to have been relatively more resistant to this deformation as only a small number of faults have been

recognized within this unit. However, calcite veins are common within this subunit between 256 and 329 mbsf. In detail, these veins consist of an outer layer of opaque white carbonate that locally grades into the carbonate wall rock, forming a recrystallized zone up to 3–4 mm wide. The central part of the veins is occupied by a later generation of translucent, gray-colored sparry calcite. This generation of sparry calcite also forms a set of later veins that postdate the polygenetic vein set.

The unconformity between lithologic Subunits IVB and VA (at 329 mbsf) is marked by a zone of intense brecciation, veining, and fracturing in Core 159-960A-37R. A fracture in Section 159-960A-37R-2 is infilled with quartzose fragments from lithologic Subunit VA in a brown carbonate matrix. Pyrite mineralization has occurred along the fracture margins. Calcite and kaolinite veins associated with pyrite are abundant below the unconformity. A typical example of a calcite-pyrite association occurs in Section 159-960A-46R-3. In this example, a syntaxial vein comprises an early generation of saw-tooth calcite overgrown by a rim of pyrite and later filled by a central zone of calcite. Calcite and pyrite also occur within a mineralized fault zone (up to 2 cm wide) at a depth of 373 mbsf.

Microfaults and associated folds in the black claystones of lithologic Unit V are associated with kaolinite veins; the latter are particularly common between 403 and 418 mbsf. Microfolds are particularly well preserved in Cores 159-960A-54R and 55R, where they are brittle, asymmetrical structures with fracturing within their hinge zones and associated with reverse microfaults. The relationship between microfaults and microfolds, especially in Cores 159-960A-54R and 55R, is described in more detail by Benkhelil et al. (Chap. 3, this volume). Kaolinite veins in lithologic Subunit VB display well-developed mineral lineations, which occur oblique to the strike of the

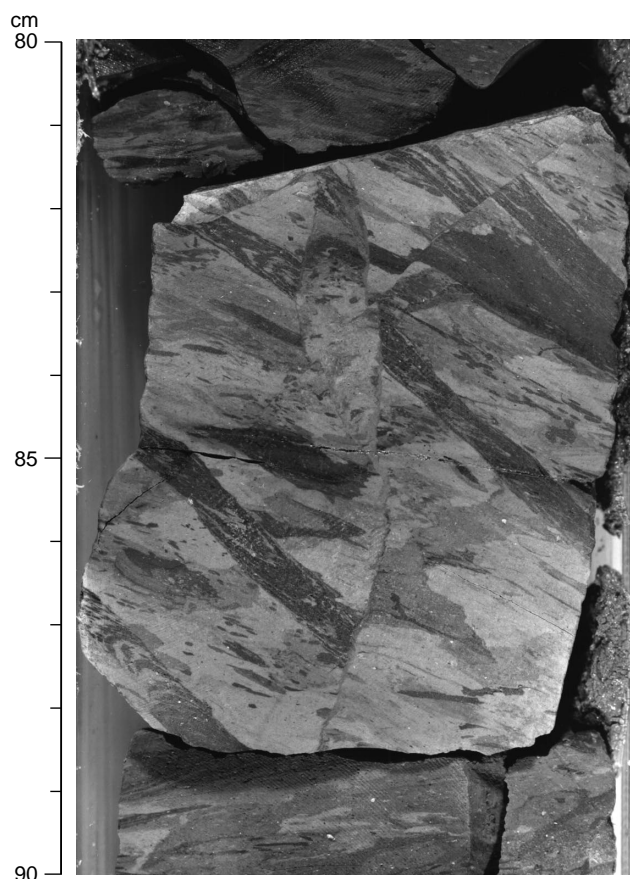


Figure 3. A subvertical, sinuous fault enclosing a lens of deformed sediment, cut by a later planar, normal fault (Section 159-959D-43R-3).

vein walls (pitch 20° – 40°), indicative of oblique slip. Further evidence for oblique slip is provided by steeply dipping fault planes in Cores 159-960A-40R and 42R (approximately 348–358 mbsf), which bear slickensides pitching 10° – 20° from strike. In one case the slickensides indicate dextral motion. The lineations and slickensides observed in lithologic Subunits VA and VB provide the most unequivocal evidence for strike slip observed on the cruise.

Site 961

Site 961 is located at latitude $3^{\circ}27'N$, longitude $3^{\circ}4'W$ in a water depth of 3303 m. It is situated on the last significant topographic expression of the Marginal Ridge; further west the ridge is obscured by the thick sedimentary cover of the Deep Ivorian Basin. Two holes were drilled (961A and 961B) with maximum penetration achieved in Hole 961B (375 mbsf).

In Hole 961A, rare, normal microfaults with offsets ≤ 1 cm were observed within lithologic Subunit IIB and Unit III between 168 and 300 mbsf. Also, within this hole an intense zone of calcite veining and fracturing was observed at 235.6 mbsf. Normal microfaulting at 285.5 mbsf (Section 159-961A-31R-CC) resulted in the development of a series of tilted blocks and horst and graben structures within the core pieces. In Hole 961B, a number of zones of brecciation and fracturing with associated calcite and pyrite mineralization were recorded between 217 and 307.5 mbsf. Within this interval, at 276 mbsf, kaolinite veins were observed within siderite concretions.

A wide variety of deformation structures was recorded in lithologic Unit III (Hole 961B) at a depth of 332–370 mbsf (Cores 159-961B-

13R through 18R), possibly representing a major zone of shearing. In Core 159-961B-13R these structures include microfolds, normal microfaults, steeply dipping shear bands, and an incipient cleavage. In thin section, this cleavage is defined by closely spaced, discontinuous seams of dark, clay-rich material. In Section 159-961B-13R-1, a vertical 2-cm-wide zone of ductile shear splays upward to form several narrower zones. Slickensides developed within the shear zone indicate that the last phase of movement was dip slip. A few vertical shear zones within lithologic Unit III display oblique slickensides, providing the only indication of a strike-slip component to the faulting (Fig. 2). A well-developed array of predominantly normal faults and shears was recorded near the base of Hole 961B within Core 159-961B-18R. In this core, a set of conjugate microfaults form a series of horst and graben structures as well as rotated fault blocks (Fig. 4). Several of these faults extend for up to 12 cm (along the length of the core) diverging into fault splays and pop-up structures. The relationship of these faults to bedding implies that they formed prior to tilting. A set of moderately dipping, dip-slip normal faults within Core 159-961B-18R display intense normal microfaulting within their footwalls. In contrast, the hanging walls of these structures display very little deformation (Fig. 4).

Site 962

Site 962 is located at latitude $3^{\circ}15'N$, longitude $3^{\circ}11'W$ in a water depth of 4650 m. It is situated on a small topographic bench that extends toward the southwest in the same direction as the Marginal Ridge southern slope. Four holes were drilled (962A, 962B, 962C, and 962D) with maximum penetration achieved in Hole 962D (394 mbsf).

In Hole 962B the claystones of lithologic Units I and II are deformed by at least one set of predominantly normal faults. In contrast, faulting within Hole 962D occurs within both the cherts of lithologic Subunit IIC and silty claystones of lithologic Unit III. In lithologic Unit III faulting is predominantly normal and commonly associated with calcite veining. In Section 159-962D-6R-CC (124 mbsf) the mineralized microfaults occur at a high angle to bedding and form a conjugate set with an angle of intersect of approximately 60° . The constant angular relationship of this conjugate fault set to bedding implies that faulting predates tilting. Calcite veins are abundant in lithologic Unit III in Hole 962D and were observed from Cores 159-962D-6R to 159-962D-37R (123–394 mbsf). These vary in morphology from single mineralized fractures to complex vein networks that commonly display up to two generations of vein fill. For example, in Section 159-962D-17R-CC (230 mbsf) an earlier set of white calcite veins are cut by a second generation of zoned veins comprising pale calcite margins and darker micritic centers. In a small number of cases, pyrite mineralization occurs within calcite veins (e.g., Section 159-962D-12R-5). Further down Hole 962D a number of calcite-filled microfaults have been observed approximately orthogonal to bedding, in particular between 288.5 mbsf and the base of the succession at 393.5 mbsf. These microfaults commonly deform the adjacent sedimentary laminations, but typically display very little offset (1 mm or less).

Several rare examples of reverse faults with associated microfolds and pop-up structures provide the only evidence for localized compression. In the siliceous rock in Core 159-962D-2R, compressional deformation resulted in the development of an open fold, with two reverse faults forming a pop-up structure in the inner hinge area. A similar geometry was observed deeper in Hole 962D (Section 159-962D-27R-CC) where microfolding in association with reverse faults also led to the development of a pop-up structure.

Evidence for strike-slip displacement is relatively rare and is found only in lithologic Unit III below approximately 300 mbsf. A small, flower-like structure displaying both normal and reverse motion in Section 159-962D-24R-3 may indicate strike-slip deforma-

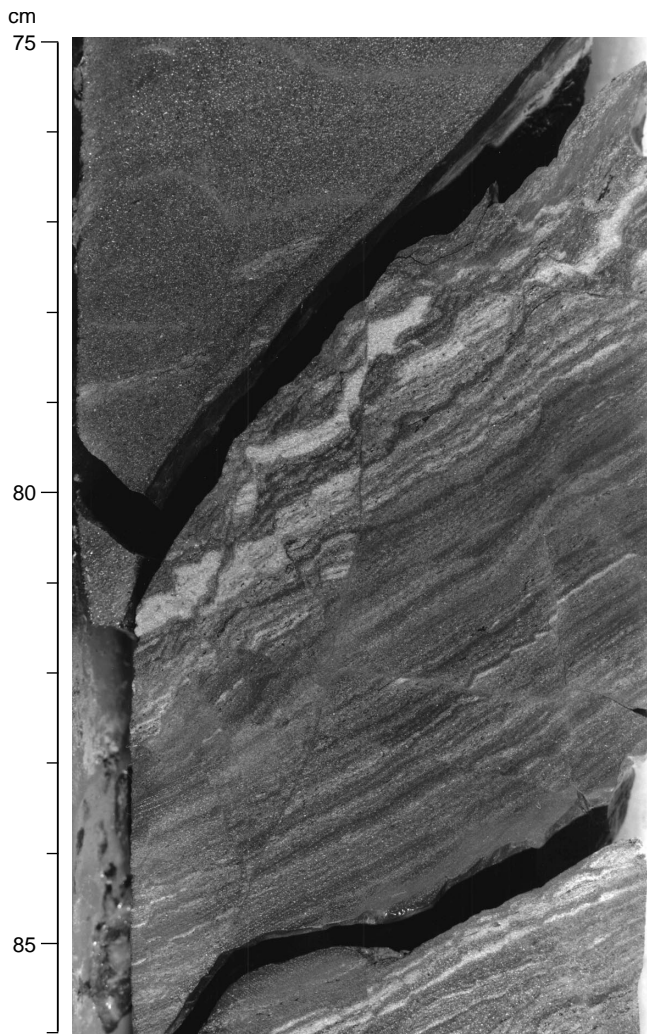


Figure 4. A set of normal microfaults forming horst and graben structures and rotated fault blocks in the footwall of a more major fault (marked by a break in the core; Section 159-961B-18R-2).

tion. A vertical fault in Section 35R-2 (376.5 mbsf) with slickensides pitching at 30° to the strike provides the only other good evidence for oblique/strike slip.

ANALYSIS OF FAULT DATA FROM SITES 959–962

With the exception of bedding surfaces, faults and mineralized faults were the most common structural features observed in the Leg 159 cores. The frequency distribution of different fault types recognized at the four sites is shown in Figure 5. Normal faults dominate at all four sites, whereas faults/fault associations displaying evidence of strike slip or oblique slip are rare. However, many of the “normal” and “reverse” faults may possess a component of oblique slip. Alternatively, these small-scale structures may form part of larger scale “flower structures” associated with strike-slip deformation (see below). The “undefined” faults may also include faults that have accommodated a significant amount of strike-slip or oblique-slip displacement. (Following the core-based studies of Lundberg and Moore [1986] lineations that pitch 70° or more have been classified as dip slip, those that pitch 20° or less strike slip, and the remainder oblique slip.) The frequency of fault dips from the four sites is shown

in Figure 6. The faults included in these plots include all fault types, including those assigned as “undefined” in Figure 5. The most common fault dips generally lie within the 40° – 60° range. Fault dips display an approximately normal frequency distribution at Site 959. The high percentage of shallow fault dips in Hole 960C may be a result of slumping of the already deformed porcellanites of lithologic Subunit IIA (especially down to 140 mbsf). If this is the case, then the angular relationship between the faults and the steeply dipping, slumped beds ($\sim 65^\circ$ – 85°), suggests an original set of moderately to steeply dipping faults. Limited fault data for Sites 961 and 962 precludes detailed analysis. The frequency data for Hole 962D reflect the large number of steeply dipping to vertical vein-filled microfaults observed at 300–400 mbsf in this hole.

Evidence for Strike Slip on Leg 159

As shown by the summary diagram of structures observed at Sites 959–960 (Fig. 2) and the histogram of fault types (Fig. 5), strike-slip faults are apparently relatively rare, and this apparent scarcity seems rather surprising given the transform margin setting. However, given the near-vertical orientation of many strike-slip faults, it is likely that they are actually much more common than indicated by core observations. This bias in favor of dip-slip faults has been noted in previous core-based structural studies (e.g., Deep Sea Drilling Project [DSDP] Leg 60 to the Mariana forearc; Lundberg and Moore, 1986). Samples of vein-filled fractures were dissected after the cruise to determine whether strike slip was more common than initially thought from shipboard observations of the core face. When broken, several samples of calcite veins (e.g., Samples 159-960A-46R-1, 98–102 cm, and 59R-01, 34–37 cm) display clear strike-slip to oblique mineral lineations, confirming that evidence for strike slip is probably more widespread in the cores than initial observations suggest.

The partitioning of strike-slip deformation into regionally discrete zones is also likely to affect the distribution of strike-slip faults observed in cores. Investigations of seismic profiles across wrench zones (e.g., Christie-Blick and Biddle, 1985) show that large strike-slip faults comprise narrow, well-defined zones in igneous or metamorphic basement at depth, grading up into zones of upward-splaying, more diffuse deformation (i.e., flower structures). Both of these fault styles are unlikely to be well recorded in cores. The higher level, splaying flower structures probably have most potential for providing structural evidence in cores and, given the depths of the holes drilled on Leg 159, are the most likely style of strike-slip motion to have been encountered. Nevertheless, many strike-slip-related associations of normal and reverse faults may appear in cores as isolated normal or reverse faults. Thus, the normal and reverse categories of Figure 5 may include structures related to strike-slip deformation on a larger scale. Also, faults that have components of both strike-slip and normal or reverse motion are likely to display the dip-slip component more obviously on the core face.

Evidence for strike-slip/oblique-slip displacement is largely confined to the Aptian–Albian sequences at Sites 960–962, whereas at Site 959 indirect evidence for strike slip was observed in younger (up to early Eocene) sediments (Fig. 2). The structures and structural associations that we took as evidence for strike slip are outlined below. We classed the evidence as “direct” or “indirect” as shown in Figure 2.

1. Strike-slip and oblique-slip slickensides/mineral lineations. Strike-slip and oblique-slip mineral lineations were observed where vein minerals (predominantly kaolinite and calcite) have grown with a clear oblique or strike-slip orientation, within the plane of the vein, perpendicular or near perpendicular to the direction of dip (e.g., well displayed in kaolinite veins in Core 159-960A-54R).

2. Vertical to subvertical, anastomosing faults and shear zones (e.g., Section 159-961B-73R-1). These faults are commonly infilled with a fine gray gouge and appear to have formed when the sediment

Figure 5. Frequency histogram showing the relative proportions of different fault types observed in cores from Sites 959–962. Faults whose offsets could not be determined on the scale of the core are classified as “undefined”. The “strike-slip” category also includes oblique-slip faults (those pitching <70° from strike).

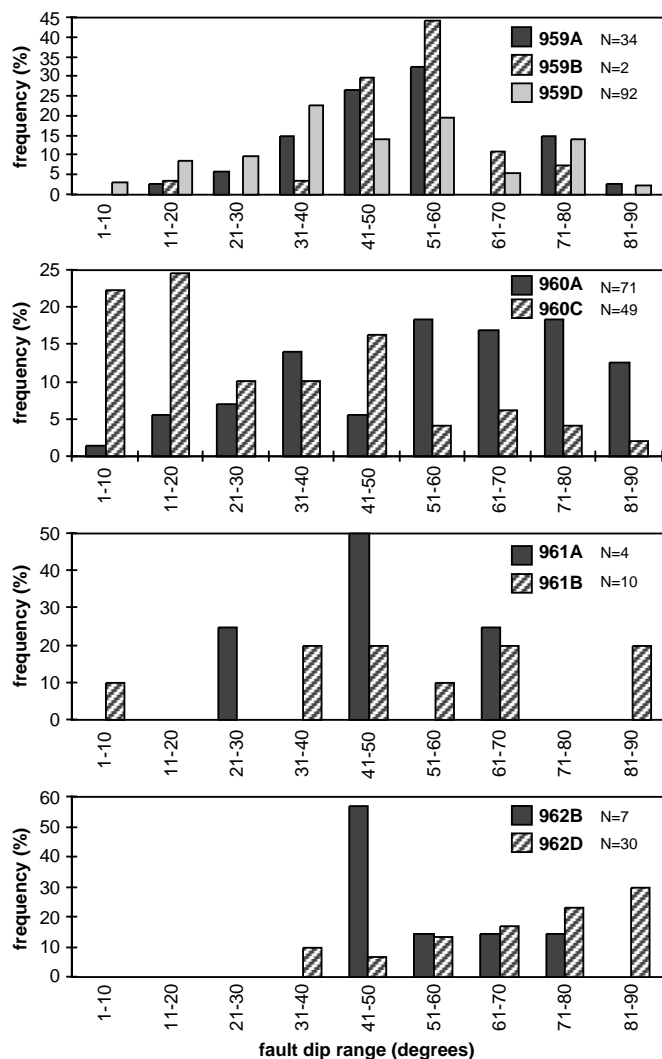
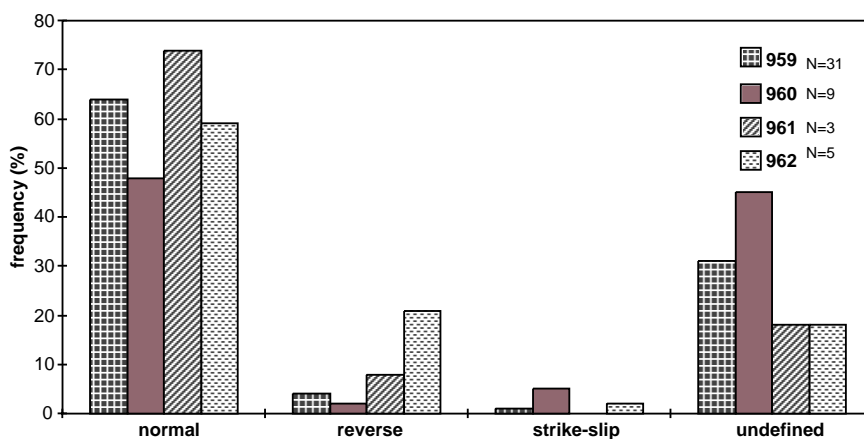


Figure 6. Frequency histograms showing the ranges of fault dips relative to horizontal in cores from Sites 959–962.

was not completely lithified. Slickensides observed along these faults are oblique, indicating a combination of dip-slip and strike-slip components. The vertical, anastomosing, and bifurcating nature of these faults is also suggestive of a significant degree of strike-slip displacement.

3. Close association of normal and reverse microfaults, possibly part of larger scale “flower” structures. Christie-Blick and Biddle (1985) described examples of such structures and recognized positive flower structures (caused by net shortening in convergent oblique zones) and negative flower structures (net extension in divergent oblique zones). Associations of reverse and normal faults are a characteristic feature of these larger structures. Seismic-scale positive flower structures have been observed in seismic reflection profiles from the Deep Ivorian Basin-Côte d’Ivoire-Ghana Marginal Ridge transition, near the Ghanaian Platform (e.g., Basile et al., 1993; Mascle et al., 1995).

4. Centimeter-scale “flower” structures of both positive and negative types (e.g., Sections 159-962D-34R-3 and 159-962D-24R-3, respectively).

ANALYSIS OF BEDDING DIPS

Bedding dips are a fundamental structural element of any sedimentary sequence, and true dips were recorded throughout the cores recovered from Leg 159.

Site 959 provides the only continuous and relatively undisturbed record of the changes in bedding dip (Fig. 7). Obviously spurious data points (i.e., ones affected by localized slumping and faulting) have been deleted from this plot. The high bedding dips recorded in the upper 100 mbsf of the succession are related to drilling disturbance and slumping. Below approximately 600 mbsf bedding dips gradually increase. A marked jump occurs at 750 mbsf, which interestingly corresponds to the point at which porosity starts to decrease downhole and faulting/veining abruptly increases. Bedding dips decrease downhole between about 1000 and 1080 mbsf (within the calcareous rocks of lithologic Subunits IVA and IVB). The unconformity between lithologic Units IV and V is marked by a sharp increase in bedding dip below the unconformity. The Site 960 bedding dip data are largely affected by slumping and faulting in the upper parts of the succession, especially in lithologic Subunit IIA (~100–140 mbsf). Variable bedding dip data below the unconformity at ~330 mbsf reflect the wide range of dips in the tectonically deformed sandstone and claystone of lithologic Unit V. Site 961 yielded relatively few data; most of it affected by slumping and faulting. Bedding dips measured at Site 962 also display widely varying values, mostly attributable to faulting and, in the interval 350–400 mbsf, possibly cross-bedding.

Rates of Tilting

Tilt rates can give a useful indication of the tectonic evolution of a sedimentary sequence, and have been used successfully on cored sequences in both backarc and forearc settings drilled on previous

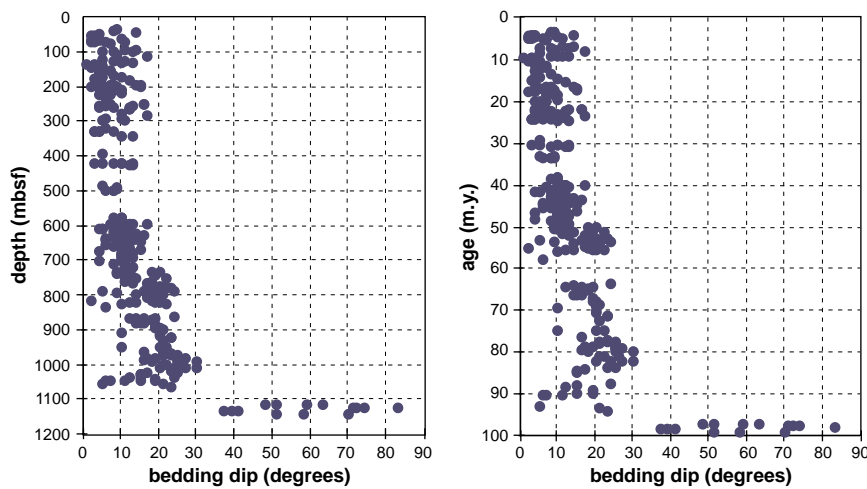


Figure 7. Bedding dip vs. depth and age for sediments recovered from Site 959. Note the high dips in the deformed Albian rocks below the unconformity at 1082 mbsf and the increase in dip at 750 mbsf (corresponding to approximately 50 Ma on the dip vs. age plot).

DSDP and ODP Legs (e.g., MacLeod, 1994; Lundberg and Moore, 1986). For Leg 159, a rough estimate of tilt rate was calculated using rates of change of average dip (Fig. 8). The method assumes a common direction of strike throughout the borehole. Evidence from the limited FMS data suggests that this is valid for the sequences above the Turonian unconformity, where the local dips in the hole generally follow the regional dip to the northwest (Masle, Lohmann, Clift, et al., 1996). Problems may occur in the sequences beneath the unconformity, where there is clear evidence for folding and major slumping. Owing to sparse bedding dip data and poor age constraints over thick sections of Sites 960, 961, and 962, tilt rates were calculated for Site 959 only. Ages were calculated for individual dip measurements using biostratigraphic data (Masle, Lohmann, Clift, et al., 1996; P.D. Clift, pers. comm., 1996) and extrapolating between known horizons. After deleting several spurious readings (anomalously high because of slumping and faulting) time brackets of 10 m.y. (5 m.y. between 90 and 100 Ma) were assigned and the average dip reading was calculated for each 10 m.y. segment. The changes between these average dips were calculated and plotted as a tilt rate (degrees per million years) from 10 to 95 Ma. From 10 to 50 Ma the tilt rate remains relatively constant at about $0.1^\circ/\text{m.y.}$, an effect that may be attributed to compaction tilting during the passive margin subsidence stage. The plot highlights the relatively high tilt rate of $0.5^\circ/\text{m.y.}$ at ~ 50 Ma, which corresponds to the obvious increase in dip observed in the bedding dip vs. age plot at this time (Fig. 7). It is noteworthy that this age corresponds closely to a depth of 750 mbsf, which also marks the level below which deformational features are most intense, as described in more detail below.

An unusual trend is also observed in the lower part of Figure 8. A tilt rate of about $0.4^\circ/\text{m.y.}$ at 70 Ma is preceded by negative tilt rates at 80 and 90 Ma (the beds at 70 Ma dip more steeply than those at 80 and 90 Ma). This may indicate that the carbonate sediments laid down at 80–90 Ma were first tilted in the opposite direction (i.e., to the southeast), and then after 70 Ma the whole sequence was tilted to the northwest. This contrasts with the inferred predominantly northward sediment transport direction based on the overall thickening and coarsening of these sediments to the south (Shipboard Scientific Party, 1996b). Alternatively, these differences in dip may be related to differential tilting associated with folding or faulting. The high tilt rate at 95 Ma corresponds to the very steep bedding dips observed below the unconformity at 1082 mbsf in Hole 959D.

DISCUSSION AND CONCLUSIONS

As summarized in Figure 2, the tectonic structures observed at Sites 959–962 include a wide range of faults, veins, and folds, displaying an overall downhole increase in intensity. Normal faults, re-

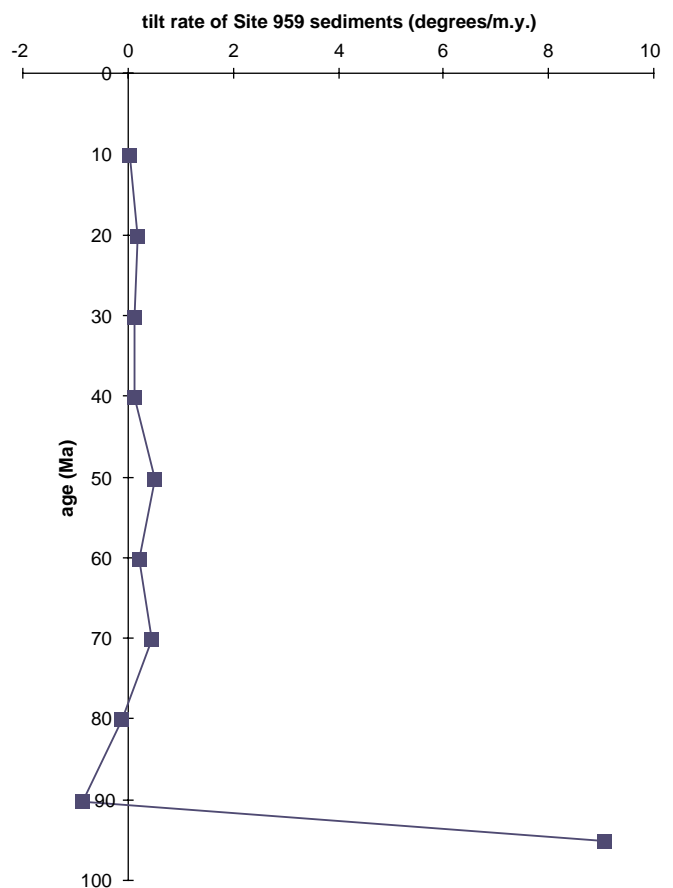


Figure 8. Plot showing tilt rate of Site 959 sediments vs. the age of the sediments.

flecting extension, are the most common fault type at all four sites. Reverse and oblique-slip/strike-slip faults are rare by comparison. In Hole 959D, normal faults can be divided into at least two generations. A steeply dipping, anastomosing set of faults was clearly postdated by sharply defined, planar faults, reflecting more lithified conditions within the transtensional regime. Reverse faulting predominantly occurs in regions of intense normal faulting, such as the black claystones in Hole 960C. Reverse faults were also observed in Hole 962D, where they are associated with normal faults in centimeter-

scale flower-type structures. Such structures may indicate strike-slip displacement and, along with rare strike-slip/oblique-slip slickensides and mineral lineations, form the main evidence for strike slip in the Leg 159 cores. Strike-slip displacement may be largely confined to narrow shear zones such as that identified between 330 and 350 mbsf in Hole 961B. Here, a 20-m-thick shear zone, characterized by a wide range of faults, microfolds, and cleavage, may represent one of the major shear zones running along the Marginal Ridge.

The scarcity of evidence for strike slip seems surprising, given the expected tectonic environment of a transform margin. Possible reasons for this have already been outlined in the text. The best evidence that we have (horizontal and near-horizontal mineral lineations and slickensides) is largely confined to Aptian–Albian sequences at Sites 960–962 (Fig. 2). This interval corresponds to the continent–continent transform phase predicted from the Equatorial Atlantic opening history. At Site 959, by contrast, we see evidence for strike slip in lithologic Unit III (Coniacian–early Eocene), which may correspond to the ocean–continent transform stage. Indirect evidence for strike-slip also occurs in lithologic Subunit IIC (Eocene). This interval of strike slip is difficult to reconcile with models for the timing of transform motion, and may represent a minor strike-slip component associated with the continued evolution of the Marginal Ridge.

Post-cruise study of data collected from Leg 159 has revealed the presence of a significant tectonic “event” in the Eocene, around 750 mbsf at Site 959 (within lithologic Subunit IIC). An increased tilt rate at Site 959 is noted at 50 Ma (early Eocene) (Fig. 8), which is approximately equivalent to the 750 mbsf depth in Hole 959D. After 50 Ma, the tilt rate is approximately constant. It is interesting that this critical point occurs in the early Eocene, supposedly within the passive transform margin stage, some 30 million years after inferred passage of the oceanic ridge along the margin.

The depth of 750 mbsf appears to record the end of major tectonic activity, as indicated by abrupt changes in bedding dip and the intensity of deformational structures. A significant change in the magnitude of index properties of the sediments (e.g., density, water content, and porosity) was also observed at about 750 mbsf. Porosity values decrease by more than 10% and density values increase by at least 0.2 g/cm³. Edwards (Chap. 22, this volume) notes that 750 mbsf represents the strongest reflector observed from the single-channel seismic data. This reflector is continuous and corresponds to a large (0.6 km/s) increase in velocity. On the flanks of the Marginal Ridge it is overlapped by overlying reflectors, an observation that fits with the change in bedding dip at this depth.

There is also evidence for a change in thermal conditions in the early Eocene. Isotopic compositions ($\delta^{18}\text{O}$) of calcite veins from Core 159-959D-36R (~750 mbsf) indicate elevated fluid temperatures, up to approximately 70°–80°C (K.C. Lohmann, pers. comm., 1996; Marcano et al., Chap. 8, this volume). A similar series of isotopically “light” veins also occurs within Albian and older sediments, below the unconformity between lithologic Units IV and V. A major phase of deformation certainly did occur before reef build-up (lithologic Unit IV) as documented by the deformed and steeply dipping nature of lithologic Unit V below the unconformity at Sites 959 and 960.

At Site 960 the early Eocene is represented by palygorskite claystones (lithologic Unit III) that lie directly above glauconitic hardgrounds (lithologic Subunit IVA) of Maastrichtian–Coniacian age. These lithologies indicate low sediment accumulation rates in a warm, marine setting (Shipboard Scientific Party, 1996c). Hardgrounds are consistent with a significant decrease in porosity and associated density and seismic velocity observed in physical properties measurements of cores and downhole logs. Following the Eocene, gradual subsidence of the transform margin to its current depth at about 2 km below sea level is evident from the deeper water facies recorded in the cores. The tilting history also indicates differential relative uplift from Campanian to Eocene times, leading to the con-

tinued development of the Marginal Ridge. After the Eocene, tilt rates are extremely low (Fig. 8) and may be related to differential compaction. This history is consistent with seismic reflection profiles, which show progressive onlap onto the ridge for horizons above 750 mbsf in Hole 959D (Masclé, Lohmann, Clift, et al., 1996).

Previous models have linked the evolution of the Marginal Ridge with the uplift caused by the thermal pulse associated with passage of a spreading ridge. Best estimates from the spreading history place the passage of the spreading ridge past the Marginal Ridge within the Late Cretaceous, about 30 m.y. before the Eocene “event”. Although there may have been some thermal lag associated with the ridge heating, this is unlikely to have lasted as long as 30 m.y.

One plausible alternative is that this Eocene event marks a switch between uncoupled and coupled linkage between the continental and oceanic crust across the transform margin. Any minor extension across the margin would lead to flexural warping of the footwall block, generating footwall uplift of the Marginal Ridge, as predicted for oceanic fracture zones (Sandwell and Schubert, 1982). Once the margin became coupled, any further differential subsidence associated with the gradual cooling and subsidence of the oceanic lithosphere would cause downwarping and subsidence of the Marginal Ridge. Cessation of active faulting along the fracture zone, coupled with continued sedimentation might have sealed active pathways for fluid circulation and limited the heating of bottom waters within the deep lithosphere. As a result, fluids would have only plumbed shallow depths, with associated lower temperatures.

If the Marginal Ridge continued to form until Eocene times, it is difficult to see how it can be associated with the passage of the spreading ridge. In fact, there is evidence from the Turonian patch reefs that the Marginal Ridge formation had commenced earlier than the Campanian age predicted from the spreading history. An origin as a flexural response to a minor component of extension across the ocean–continental margin may prove to be a more plausible mechanism for the development of the Marginal Ridge.

ACKNOWLEDGMENTS

This work was undertaken at the University of Edinburgh during postcruise research funded by NERC. The British Geological Survey (NERC) is thanked for allowing EAP to attend the postcruise meeting. We thank Peter Clift, Rosemary Edwards, Kacey Lohmann, Roger Scrutton and Emrys Phillips for advice and useful discussions. Alastair Robertson and two anonymous reviewers are thanked for their reviews and comments.

REFERENCES

- Basile, C., Masclé, J., Popoff, M., Bouillin, J.P., and Masclé, G., 1993. The Côte d'Ivoire-Ghana transform margin: a marginal ridge structure deduced from seismic data. *Tectonophysics*, 222:1–19.
- Christie-Blick, N., and Biddle, K.T., 1985. Deformation and basin formation along strike-slip faults. In Biddle, K.T., and Christie-Blick, N. (Eds.), *Strike-slip Deformation, Basin Formation and Sedimentation*. Spec. Publ.—Soc. Econ. Paleontol. Mineral., 37:1–34.
- Crowell, J.C., 1974. Origin of late Cenozoic basins in southern California. In Dickinson, W.R. (Ed.), *Tectonics and Sedimentation*. Spec. Publ.—Soc. Econ. Paleontol. Mineral., 22:190–204.
- Kopf, A., and Flecker, R., 1996. Problems associated with the interpretation of normal fault distributions in sediments recovered by the advanced hydraulic piston corer during Leg 160, Eastern Mediterranean. In Emeis, K.-C., Robertson, A.H.F., Richter, C., et al., *Proc. ODP, Init. Repts.*, 160: College Station, TX (Ocean Drilling Program), 507–511.
- Lundberg, N., and Moore, J.C., 1986. Macroscopic structural features in Deep Sea Drilling Project cores from forearc regions. In Moore, J.C. (Ed.), *Structural Fabric in Deep Sea Drilling Project Cores From Forearcs*. Mem.—Geol. Soc. Am., 166:13–44.

- MacLeod, C.J., 1994. Structure of the outer Tonga forearc at Site 841. In Hawkins, J., Parson, L., Allan, J., et al., *Proc. ODP, Sci. Results*, 135: College Station, TX (Ocean Drilling Program), 313–329.
- Masclé, J., Basile, C., Pontoise, B., and Sage, F., 1995. The Côte d'Ivoire-Ghana transform margin: an example of an ocean-continent transform boundary. In Banda, E., Talwani, M., and Thorne, M. (Eds.), *Rifted Ocean-Continent Boundaries*, NATO ASI Ser.: Dordrecht (Kluwer), 327–339.
- Masclé, J., and Blarez, E., 1987. Evidence for transform margin evolution from the Côte d'Ivoire-Ghana continental margin. *Nature*, 326:378–381.
- Masclé, J., Lohmann, G.P., Clift, P.D., et al., 1996. *Proc. ODP, Init. Repts.*, 159: College Station, TX (Ocean Drilling Program).
- Sandwell, D.T., and Schubert, G., 1982. Lithospheric flexure at fracture zones. *J. Geophys. Res.*, 87:4657–4667.
- Shipboard Scientific Party, 1996a. Explanatory notes. In Masclé, J., Lohmann, G.P., Clift, P.D., et al., *Proc. ODP, Init. Repts.*, 159: College Station, TX (Ocean Drilling Program), 17–46.
- , 1996b. Principal results. In Masclé, J., Lohmann, G.P., Clift, P.D., et al., *Proc. ODP, Init. Repts.*, 159: College Station, TX (Ocean Drilling Program), 297–314.
- , 1996c. Site 960. In Masclé, J., Lohmann, G.P., Clift, P.D., et al., *Proc. ODP, Init. Repts.*, 159: College Station, TX (Ocean Drilling Program), 151–215.

Date of initial receipt: 19 September 1996

Date of acceptance: 27 May 1997

Ms 159SR-002